

---

# Sparse within Sparse Gaussian Processes using Neighbor Information

---

**Gia-Lac Tran**  
Eurecom

**Dimitrios Milios**  
Eurecom

**Pietro Michiardi**  
Eurecom

**Maurizio Filippone**  
Eurecom

## Abstract

Approximations to Gaussian processes (GPs) based on inducing variables, combined with variational inference techniques, enable state-of-the-art sparse approaches to infer GPs at scale through mini-batch-based learning. In this work, we address one limitation of sparse GPs, which is due to the challenge in dealing with a large number of inducing variables without imposing a special structure on the inducing inputs. In particular, we introduce a novel hierarchical prior, which imposes sparsity on the set of inducing variables. We treat our model variationally, and we experimentally show considerable computational gains compared to standard sparse GPs when sparsity on the inducing variables is realized considering the nearest inducing inputs of a random mini-batch of the data. We perform an extensive experimental validation that demonstrates the effectiveness of our approach compared to the state-of-the-art. Our approach enables the possibility to use sparse GPs using a large number of inducing points without incurring a prohibitive computational cost.

## 1 INTRODUCTION

Gaussian Processes (GPs) (Rasmussen and Williams, 2006) offer a powerful framework to perform inference over functions; being Bayesian, GPs provide rigorous uncertainty quantification and prevent overfitting. However, the applicability of GPs on big datasets is hindered by their computational complexity of  $\mathcal{O}(N^3)$ , where  $N$  is the training size. This issue has fuelled a considerable amount of research towards scalable GP methodologies

that operate on a set of *inducing variables* (Quiñonero Candela and Rasmussen, 2005). In the literature, there is a plethora of approaches that offer different treatments of the inducing variables (Lawrence et al., 2002; Seeger et al., 2003; Snell and Ghahramani, 2005; Naish-Guzman and Holden, 2007; Titsias, 2009; Hensman et al., 2013; Wilson and Nickisch, 2015; Hensman et al., 2015). Some of the more recent approaches, such as Scalable Variational Gaussian Processes (SVGPs) (Hensman et al., 2015), allow for the application of GPs to problems with millions of data points. In most applications of scalable GPs, these are approximated using  $M$  inducing points, which results in a complexity of  $\mathcal{O}(M^3)$ . It has been shown recently by Burt et al. (2019) that it is possible to obtain an arbitrarily good approximation for a certain class of GP models (i.e. conjugate likelihoods, concentrated distribution for the training data) with  $M$  growing more slowly than  $N$ . However, the general case remains elusive and it is still possible that the required value for  $M$  may exceed a certain computational budget. Our result contributes to strengthen our belief that sparsity does not only enjoy desirable theoretical properties, but it also constitutes an extremely computationally efficient method in practice.

In this work, we push the limits of scalability and effectiveness of sparse GPs enabling a further reduction in complexity, which can be translated to higher accuracy by considering a larger set of inducing variables. The idea is to operate on a subset of  $H$  inducing points during training and prediction, with  $H \ll M$ , while maintaining a sparse approximation with  $M$  inducing variables. We formalize our strategy by imposing a sparsity-inducing structure on the prior over the inducing variables and by carrying out a variational formulation of this model. This extends the original SVGP framework and enables mini-batch-based optimization for the variational objective. We then consider ways to select the set of  $H$  inducing points based on neighbor information; at training time, for a given mini-batch, we activate  $H$  out of  $M$  inducing variables considering the nearest inducing inputs to the samples in the mini-batch, whereas at test time we select inducing variables

corresponding to the inducing inputs which are nearest to the test data-points. We name our proposal *Sparse within a Sparse GP* (SWSGP). SWSGP is characterized by a number of attractive features: (i) it improves significantly the prediction quality using a small number of neighboring inducing inputs, and (ii) it accelerates the training phase, especially when the total number of inducing points becomes large. We extensively validate these properties on a variety of regression and classification tasks. We also showcase SWSGP on a large scale classification problem where we set  $M = 100,000$ ; we are not aware of other approaches that can handle such a large set of inducing inputs without imposing some special structure on them (e.g., grid) or without considering one-dimensional inputs.

Hierarchical priors are often applied in Bayesian modeling to achieve compression and to improve flexibility (Molchanov et al., 2017; Louizos et al., 2017). To the best of our knowledge, this work is the first to explore these ideas for the purposes of sparsifying the inducing set in sparse GPs.

## 2 RELATED WORK AND BACKGROUND

Sparse GPs that operate on inducing inputs have been extensively studied in the last 20 years (Csató and Opper, 2002; Lawrence et al., 2002; Snelson and Ghahramani, 2005; Quiñonero Candela and Rasmussen, 2005; Naish-Guzman and Holden, 2007). Many attempts on sparse GPs specified inducing inputs by satisfying certain criteria that produce an informative set of inducing variables (Csató and Opper, 2002; Lawrence et al., 2002; Seeger et al., 2003). A different treatment has been proposed by Titsias (2009), which involves formulating the selection of inducing inputs as optimization of a variational lower bound to the marginal likelihood. The variational framework was later expanded so that stochastic optimization can be admitted, thus improving scalability for regression (Hensman et al., 2013) and classification (Hensman et al., 2015). In a more recent work (Panos et al., 2018) scalability is addressed in terms of the dimensionality of the input. All the aforementioned methodologies share a computational complexity of  $\mathcal{O}(M^3)$ . Although there have been some attempts in the literature to infer the appropriate number of inducing points as well as the inducing inputs (Pourhabib et al., 2014; Burt et al., 2019), a large number of inducing variables is desirable in improving the approximation to the posterior. In this work we present a methodology that builds on the SVGP framework (Hensman et al., 2015) and reduces its complexity, thus increasing the potential of sparse GP application on even larger datasets and with a larger

set of inducing variables.

A different approach to scalable GPs was introduced by Wilson and Nickisch (2015), namely Kernel Interpolation for Scalable Structured GPs (KISS-GP). This line of work involves arranging a large number of inducing inputs into a grid structure; this allows one to scale to very large datasets by means of fast linear algebra. The applicability of KISS-GP on higher-dimensional problems has been addressed by Wilson et al. (2015) by means of low-dimensional projections. A more recent extension allows for a constant-time variance prediction using Lanczos methods (Pleiss et al., 2018). Our work takes a different approach by keeping the GP prior intact, and by imposing sparsity on the set of inducing variables.

Local approximation of GPs inspired by the the concept of divide-and-conquer is also a practical solution to implement scalable GPs (Kim et al., 2005; Urtasun and Darrell, 2008; Datta et al., 2016; Park and Huang, 2016; Park and Apley, 2017) which allows GPs to work on large-scale datasets. In our work, we use neighbour information in a different way, by incorporating it in a certain hierarchical structure of the auxiliary variables through a variational scheme.

### 2.1 Scalable Variational Gaussian Processes

Consider a supervised learning problem with inputs  $\mathbf{X} = (\mathbf{x}_1, \dots, \mathbf{x}_N)^\top$  associated with labels  $\mathbf{y} = (y_1, \dots, y_N)^\top$ . Given a set of latent variables  $\mathbf{f} = (f_1, \dots, f_N)^\top$ , GP models assume that labels are stochastic realizations based on  $\mathbf{f}$  and a likelihood function  $p(\mathbf{y} | \mathbf{f})$ . In SVGP, the set of inducing points is characterized by inducing inputs  $\mathbf{Z} = (\mathbf{z}_1, \dots, \mathbf{z}_M)^\top$  and inducing variables  $\mathbf{u} = (u_1, \dots, u_M)^\top$ . Regarding  $\mathbf{f}$  and  $\mathbf{u}$ , we have the following joint prior:

$$p(\mathbf{f}, \mathbf{u}) = \mathcal{N}\left(0, \begin{bmatrix} \mathbf{K}_\mathbf{X} & \mathbf{K}_{\mathbf{X}, \mathbf{Z}} \\ \mathbf{K}_{\mathbf{Z}, \mathbf{X}} & \mathbf{K}_\mathbf{Z} \end{bmatrix}\right), \quad (1)$$

where  $\mathbf{K}_\mathbf{X}$ ,  $\mathbf{K}_\mathbf{Z}$  and  $\mathbf{K}_{\mathbf{X}, \mathbf{Z}}$  are covariance matrices evaluated at the inputs indicated by the subscripts. The posterior over inducing variables is approximated by a variational distribution  $q(\mathbf{u}) = \mathcal{N}(\mathbf{u} | \mathbf{m}, \mathbf{S})$ , while keeping the exact conditional  $p(\mathbf{f} | \mathbf{u})$  intact, that is  $q(\mathbf{f}, \mathbf{u}) = p(\mathbf{f} | \mathbf{u})q(\mathbf{u})$ . The variational parameters  $\mathbf{m}$  and  $\mathbf{S}$ , as well as the inputs  $\mathbf{Z}$ , are optimized by maximizing a lower bound on the marginal likelihood  $p(\mathbf{y} | \mathbf{X}) = \int p(\mathbf{y} | \mathbf{f})p(\mathbf{f} | \mathbf{X})d\mathbf{f}$ . The lower bound on  $\log p(\mathbf{y} | \mathbf{X})$  can be obtained by considering the form of  $q(\mathbf{f}, \mathbf{u})$  above and by applying Jensen's inequality:

$$E_{q(\mathbf{f})} \log p(\mathbf{y} | \mathbf{f}) - \text{KL}(q(\mathbf{u}) \| p(\mathbf{u})). \quad (2)$$

The approximate posterior  $q(\mathbf{f})$  can be computed by integrating out  $\mathbf{u}$ :  $q(\mathbf{f}) = \int q(\mathbf{u})p(\mathbf{f} | \mathbf{u})d\mathbf{u}$ . Thanks

to the Gaussian form of  $q(\mathbf{u})$ ,  $q(\mathbf{f})$  can be computed analytically:

$$q(\mathbf{f}) = \mathcal{N}(\mathbf{f} \mid \mathbf{A}\mathbf{m}, \mathbf{K}_\mathbf{X} + \mathbf{A}(\mathbf{S} - \mathbf{K}_\mathbf{Z})\mathbf{A}), \quad (3)$$

where  $\mathbf{A} = \mathbf{K}_{\mathbf{X},\mathbf{Z}}\mathbf{K}_\mathbf{Z}^{-1}$ . When the likelihood factorizes over training points, the lower bound can be re-written as:

$$\sum_{i=1}^N \mathbb{E}_{q(f_i)} [\log p(y_i \mid f_i)] - \text{KL}(q(\mathbf{u}) \parallel p(\mathbf{u})). \quad (4)$$

Each term of the one-dimensional expectation of the log-likelihood can be computed by Gauss-Hermite quadrature for any likelihoods (and analytically for the Gaussian likelihood). The  $\text{KL}(q(\mathbf{u}) \parallel p(\mathbf{u}))$  term can be computed analytically given that  $q(\mathbf{u})$  and  $p(\mathbf{u})$  are both Gaussian. To maintain positive-definiteness of  $\mathbf{S}$  and perform unconstrained optimization,  $\mathbf{S}$  is parametrized as  $\mathbf{S} = \mathbf{L}\mathbf{L}^T$ , with  $\mathbf{L}$  lower triangular.

### 3 SPARSE WITHIN SPARSE GP

We present a novel formulation of sparse GPs, which permits the use of a random subset of the inducing points with little loss in performance. We introduce a set of binary random variables  $\mathbf{w} \in \{0, 1\}^M$  to govern the inclusion of inducing inputs  $\mathbf{Z}$  and the corresponding variables  $\mathbf{u}$ . We then employ these random variables to define a hierarchical structure on the prior as follows:

$$p(\mathbf{u} \mid \mathbf{w}) = \mathcal{N}(\mathbf{0}, \mathbf{D}_\mathbf{w}\mathbf{K}_\mathbf{Z}\mathbf{D}_\mathbf{w}), \quad (5)$$

where  $\mathbf{D}_\mathbf{w} = \text{diag}(\mathbf{w})$ , and  $\mathbf{w} \sim p(\mathbf{w})$ . Although the marginalized prior  $p(\mathbf{u})$  is not Gaussian, it is possible to use the joint  $p(\mathbf{u}, \mathbf{w}) = p(\mathbf{u} \mid \mathbf{w})p(\mathbf{w})$  within a variational scheme. We thus consider a random subset of the inducing points during the evaluation of the prior in the variational scheme that follows; no inducing points are permanently removed. Regarding  $p(\mathbf{w})$ , we consider an implicit distribution: its analytical form is unknown, but we can draw samples from it. Later, we will consider  $p(\mathbf{w})$  based on the nearest inducing inputs to random mini-batches of data.

**Remarks on the prior over  $\mathbf{f}$**  Our strategy simply assumes a certain structure on the auxiliary variables, but it *has no effect* on the prior over  $\mathbf{f}$ ; the latter remains unchanged. Let  $\mathcal{I}$  and  $\mathcal{J}$  be the sets of indices such that  $\mathbf{w}_\mathcal{I} = \mathbf{1}$  and  $\mathbf{w}_\mathcal{J} = \mathbf{0}$ . Given an appropriate ordering, the conditional  $\mathbf{u} \mid \mathbf{w}$  is effectively the element-wise product  $[\mathbf{u}_\mathcal{I}, \mathbf{u}_\mathcal{J}]^\top = \mathbf{u} \circ \mathbf{w}$ . This reduces the variances and covariances of some elements of  $\mathbf{u}$  to zero yielding a distribution of this form:

$$p(\mathbf{f}, \mathbf{u} \mid \mathbf{w}) = \mathcal{N}\left(\begin{bmatrix} \mathbf{0} \\ \mathbf{0} \\ \mathbf{0} \end{bmatrix}, \begin{bmatrix} \mathbf{K}_\mathbf{X} & \mathbf{K}_{\mathbf{X},\mathbf{Z}_\mathcal{I}} & \mathbf{0} \\ \mathbf{K}_{\mathbf{Z}_\mathcal{I},\mathbf{X}} & \mathbf{K}_{\mathbf{Z}_\mathcal{I}} & \mathbf{0} \\ \mathbf{0} & \mathbf{0} & \mathbf{0} \end{bmatrix}\right) \quad (6)$$

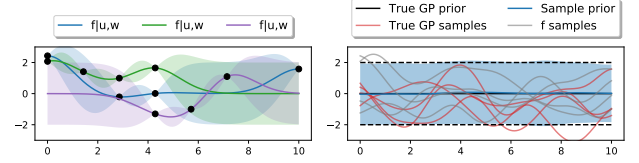


Figure 1: The choice of inducing points does not affect the prior samples drawn from  $p(\mathbf{f})$ . Left: visualizations of  $\mathbf{f} \mid \mathbf{u}, \mathbf{w}$  for different samples of  $\mathbf{w}$ . Right: comparison of the marginalised (w.r.t.  $\mathbf{u}, \mathbf{w}$ ) prior over  $\mathbf{f}$ , against the true  $p(\mathbf{f})$ .

The rows and columns of  $\mathbf{u}_\mathcal{J}$  can simply be ignored. Regardless of the value of  $\mathbf{w}$ , the conditional  $\mathbf{f}, \mathbf{u}_\mathcal{I} \mid \mathbf{w}$  is always a Gaussian marginal, as it is a subset of Gaussian variables. The marginalized  $p(\mathbf{f}, \mathbf{u}) = \int p(\mathbf{f}, \mathbf{u} \mid \mathbf{w})p(\mathbf{w})d\mathbf{w}$  is mixture of Gaussian densities, where the marginal over  $\mathbf{f}$  is the same for every component of the mixture.

The effect on  $\mathbf{f}$  is demonstrated in Figure 1, where we sample from the (non-Gaussian) marginalized prior  $p(\mathbf{u})$  in two steps: first we consider an arbitrary random subset  $\mathbf{u}_\mathcal{I}$ , and then we sample from  $p(\mathbf{u}_\mathcal{I}) \equiv p(\mathbf{u} \mid \mathbf{w})$ . Finally,  $\mathbf{f}$  samples are drawn from  $p(\mathbf{f} \mid \mathbf{u}_\mathcal{I})$ , which only involves the selected inducing variables  $\mathbf{u}_\mathcal{I}$ . Following Eq. (1), the conditional  $\mathbf{f} \mid \mathbf{u}$  is normally-distributed with mean  $\mathbf{m}_{\mathbf{f} \mid \mathbf{u}_\mathcal{I}} = \mathbf{K}_{\mathbf{X},\mathbf{Z}_\mathcal{I}}\mathbf{K}_{\mathbf{Z}_\mathcal{I}}^{-1}\mathbf{u}_\mathcal{I}$  and covariance  $\mathbf{S}_{\mathbf{f} \mid \mathbf{u}_\mathcal{I}} = \mathbf{K}_\mathbf{X} - \mathbf{K}_{\mathbf{X},\mathbf{Z}_\mathcal{I}}\mathbf{K}_{\mathbf{Z}_\mathcal{I}}^{-1}\mathbf{K}_{\mathbf{Z}_\mathcal{I},\mathbf{X}}$ . These conditionals can be seen for different samples of  $\mathbf{u}, \mathbf{w}$  in the left side of Figure 1, while in the right side we compare the marginalized prior over  $\mathbf{f}$  against the true GP prior.

Of course, although the prior remains unchanged, that is not the case for the posterior approximation. It is well known that the choice of inducing inputs has an effect on the variational posterior (Titsias, 2009; Burt et al., 2019). Our choice to impose a hierarchical structure to the inducing variables through  $\mathbf{w}$  effectively changes the model compared to SVGP, and we adapt the variational scheme accordingly.

#### 3.1 Lower bound on marginal likelihood

By introducing  $\mathbf{u}, \mathbf{w}$  and using Jensen's inequality, the lower bound on  $\log p(\mathbf{y})$  can be obtained as follows

$$\mathbb{E}_{q(\mathbf{u}, \mathbf{w})} \log p(\mathbf{y} \mid \mathbf{u}, \mathbf{w}) - \text{KL}(q(\mathbf{u}, \mathbf{w}) \parallel p(\mathbf{u}, \mathbf{w})), \quad (7)$$

where we choose the variational distribution  $q$  to reflect the hierarchical structure of the prior, i.e.  $q(\mathbf{u}, \mathbf{w}) = q(\mathbf{u} \mid \mathbf{w})p(\mathbf{w})$ . This choice enforces sparsity over the approximate posterior  $q$ ; the variational parameters are shared among the conditionals  $q(\mathbf{u} \mid \mathbf{w})$ , for which we assume:

$$q(\mathbf{u} \mid \mathbf{w}) = \mathcal{N}(\mathbf{u} \mid \mathbf{D}_\mathbf{w}\mathbf{m}, \mathbf{D}_\mathbf{w}\mathbf{S}\mathbf{D}_\mathbf{w}) \quad (8)$$

By maximizing the variational bounds that follow, we impose a  $q$  that performs well under a sparsified inducing set. We continue by applying Jensen's inequality on  $p(\mathbf{y}|\mathbf{u}, \mathbf{w})$ , obtaining:

$$\log p(\mathbf{y}|\mathbf{u}, \mathbf{w}) \geq \mathbb{E}_{p(\mathbf{f}|\mathbf{u}, \mathbf{w})} \log p(\mathbf{y}|\mathbf{f}) \quad (9)$$

We can now substitute (9) into (7), obtaining a bound where we expand  $q(\mathbf{u}, \mathbf{w})$  as  $q(\mathbf{u}|\mathbf{w})p(\mathbf{w})$ . By making this assumption, we obtain the following evidence lower bound  $\mathcal{L}_{\text{ELBO}}$ :

$$\sum_{n=1}^N \mathbb{E}_{p(\mathbf{w})} \left[ \mathbb{E}_{q(\mathbf{u}|\mathbf{w})} \mathbb{E}_{p(f_n|\mathbf{u}, \mathbf{w})} \log p(y_n|f_n) - \frac{1}{N} \text{KL} \left( q(\mathbf{u}|\mathbf{w}) \middle\| p(\mathbf{u}|\mathbf{w}) \right) \right] \quad (10)$$

Recall that  $p(\mathbf{w})$  is implicit: although we do not make any particular assumptions about its analytical form, we can draw samples from it. Using MC sampling from  $p(\mathbf{w})$ , we can obtain the approximation  $\tilde{\mathcal{L}}_{\text{ELBO}}$ :

$$\sum_{n=1}^N \left[ \mathbb{E}_{q(\mathbf{u}|\tilde{\mathbf{w}}^{(n)})} \mathbb{E}_{p(f_n|\mathbf{u}, \tilde{\mathbf{w}}^{(n)})} \log p(y_n|f_n) - \frac{1}{N} \text{KL} \left( q(\mathbf{u}|\tilde{\mathbf{w}}^{(n)}) \middle\| p(\mathbf{u}|\tilde{\mathbf{w}}^{(n)}) \right) \right], \quad (11)$$

where  $\tilde{\mathbf{w}}^{(n)}$  is sampled from  $p(\mathbf{w})$ .

**Sampling from the set of inducing points.** Recall that any sample  $\tilde{\mathbf{w}}$  from  $p(\mathbf{w})$  is a binary vector, i.e.  $\mathbf{w} \in \{0, 1\}^M$ . In case all elements of  $\mathbf{w}$  are set to one, our approach recovers the original SVGP with computational cost of  $\mathcal{O}(M^3)$  coming from computing  $p(f_n|\mathbf{u}, \tilde{\mathbf{w}} = \mathbf{1})$  and  $\text{KL}(q(\mathbf{u}|\mathbf{w}) \| p(\mathbf{u}|\mathbf{w}))$  in the ELBO. When a  $\tilde{w}_i$  is set to zero, the entries of the  $i$ -th row and  $i$ -th column of the covariance matrix in  $p(\mathbf{u}|\mathbf{w})$  and  $q(\mathbf{u}|\mathbf{w})$  are zero. This means that the  $i$ -th variable becomes unnecessary, so we get rid of  $i$ -th row and column in these matrices, and also eliminate the  $i$ -th element in mean vectors of  $q(\mathbf{u}|\mathbf{w})$  and  $p(\mathbf{u}|\mathbf{w})$ . This is equivalent to selecting a set of active inducing points in each training iteration.

### 3.2 H-nearest inducing inputs

Despite the fact that  $p(\mathbf{w})$  is an implicit distribution, we have been able to define and calculate a variational bound, assuming we can sample from  $p(\mathbf{w})$ . We shall now describe our sampling strategy, which relies on neighbor information of random mini-batches.

In order to explain the idea conveniently, we introduce  $\mathbf{Z}_{\mathbf{x}}^H$  as the set of  $H$ -nearest inducing inputs. Intuitively, the prediction for an unseen data  $\mathbf{x}$  using  $\mathbf{Z}_{\mathbf{x}}^H$  is a good approximation of the prediction using all  $M$  inducing

points, that is  $\mathbf{Z}_{\mathbf{x}}^M$ . This can be verified by looking at the predictive mean, which is expressed as a linear combination of kernel functions evaluated between training points and a test point, as in Eq. (3). The majority of the contribution is given by the inducing points with the largest kernel values, so we can use this as a criterion to establish whether an inducing input is “close” to an input vector (the effect of different kernels on the definition of nearest neighbors is explored in the supplement). With this intuition,  $p(\mathbf{w})$  becomes a deterministic function  $w(\mathbf{x})$  indicating which inducing inputs are activated. For mini-batch-based training, the value of  $\mathbf{w}$  remains random, as it depends on the elements  $\mathbf{x}$  that are selected in the random mini-batch; this materializes the sampling from the implicit distribution  $p(\mathbf{w})$ . The maximization of the ELBO in the setting described is summarized in Algorithm 1 (swsgp). At test time, however, the inputs of interest

**Algorithm 1** Sparse within sparse GP (swsgp).

**Input:**  $\mathcal{D}, H, M$ .

**Result:** The optimum of trainable parameters  $\theta$ .

```

1: Initialize  $\theta$ , i.e. kernel's parameters,  $\mathbf{Z}$ ,  $\mathbf{m}$  and  $\mathbf{S}$ .
2: while stopping criteria is False do
3:    $\text{ELL} \leftarrow 0$  and  $\text{KL} \leftarrow 0$ .
4:   Sample mini-batch  $\mathcal{I}$  of size  $n$  from  $\mathcal{D}$ .
5:   for  $(\mathbf{x}_i, y_i) \in \mathcal{I}$  do
6:     Find  $\mathbf{Z}_{\mathbf{x}_i}^H$ , i.e. the  $H$ -nearest  $\mathbf{Z}$  to  $\mathbf{x}_i$ .
7:     Compute  $w(\mathbf{x}_i)$  using  $\mathbf{Z}_{\mathbf{x}_i}^H$  as in (12)
8:     Extract  $\mathbf{m}_{w(\mathbf{x}_i)}$  and  $\mathbf{S}_{w(\mathbf{x}_i)}$  from  $\mathbf{m}$  and  $\mathbf{S}$ .
9:     Compute  $q(f_i|w(\mathbf{x}_i))$  as in (13).
10:     $\text{ELL} \leftarrow \text{ELL} + \mathbb{E}_{q(f_i|w(\mathbf{x}_i))} \log p(y_i|f_i)$ .
11:     $\text{KL} \leftarrow \text{KL} + \text{KL}(q(\mathbf{u}_{w(\mathbf{x}_i)}) \| p(\mathbf{u}_{w(\mathbf{x}_i)}))$ 
12:   end for
13:    $\tilde{\mathcal{L}}_{\text{ELBO}} \leftarrow \frac{N}{n} \text{ELL} - \frac{1}{n} \text{KL}$ .
14:   Update  $\theta$  using the derivative of  $\tilde{\mathcal{L}}_{\text{ELBO}}$ .
15: end while

```

are not random; we need to describe the predictive distribution in terms of the deterministic function  $w(\mathbf{x})$ . In fact, if we would like to approximate the predictive distribution at  $\mathbf{x}_n$  using  $H$ -nearest inducing inputs to  $\mathbf{x}$ , i.e.  $\mathbf{Z}_{\mathbf{x}_n}^H$ , then  $w(\mathbf{x}) = [w_{\mathbf{x}}^{(1)} \dots w_{\mathbf{x}}^{(M)}]^T$  where,

$$w_{\mathbf{x}}^{(m)} = \begin{cases} 1 & \text{if } \mathbf{z}_m \in \mathbf{Z}_{\mathbf{x}}^H \\ 0 & \text{else} \end{cases}, \text{ with } m = 1, \dots, M \quad (12)$$

We extract the relevant elements using  $w(\mathbf{x})$ ; for the mean, we have  $\mathbf{m}_{w(\mathbf{x}_i)} = \mathbf{D}_{w(\mathbf{x}_i)} \mathbf{m}$ , and for the covariance we select the appropriate rows and columns using  $\mathbf{S}_{w(\mathbf{x}_i)} = \mathbf{D}_{w(\mathbf{x}_i)} \mathbf{S} \mathbf{D}_{w(\mathbf{x}_i)}$ . The approximate posterior

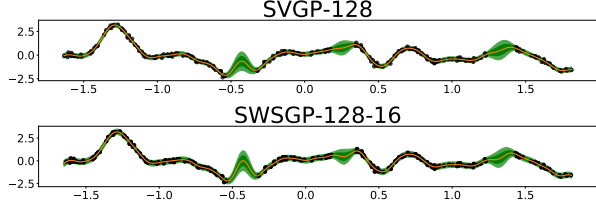


Figure 2: Visualization of posterior distribution of SVGP and SWSGP. In both cases, we consider 128 inducing points; in terms of our scheme (SWSGP) we use 16 neighbors.

over  $f_i$  given  $w(\mathbf{x}_i)$ , i.e.  $q(f_i | w(\mathbf{x}_i))$  is:

$$\mathcal{N}\left(f_i | \mathbf{A}_{\mathbf{x}_i} \mathbf{m}_{w(\mathbf{x}_i)}, \mathbf{K}_{\mathbf{x}_i} + \mathbf{A}_{\mathbf{x}_i} \left( \mathbf{S}_{w(\mathbf{x}_i)} - \mathbf{K}_{\mathbf{Z}_{\mathbf{x}_i}^H} \right) \mathbf{A}_{\mathbf{x}_i}^\top\right), \quad (13)$$

where  $\mathbf{A}_{\mathbf{x}_i} = \mathbf{K}_{\mathbf{x}_i, \mathbf{Z}_{\mathbf{x}_i}^H} \mathbf{K}_{\mathbf{Z}_{\mathbf{x}_i}^H}^{-1}$ .

**One-dimensional regression example.** We visualize the posterior distribution for a synthetic dataset generated on a one-dimensional input space. We execute SVGP and SWSGP, and depict the posterior distributions of these two methods by showing the predictive means (orange lines) and the 95% credible intervals (shaded areas) in Figure 2. We consider identical settings for the two methods (i.e. 128 inducing points, kernel parameters, likelihood variance) and a neighbor area of 16 for SWSGP; a full account of the setup can be found in the supplement. We see that although the models are different, the predictive distributions appear remarkably similar. A more extensive evaluation follows in Section 4.

### 3.3 Complexity

The computational cost of SWSGP is dominated by lines 6, 8 and 9 in Algorithm 1. For each data point  $(\mathbf{x}_i, y_i)$  in mini-batch  $\mathcal{I}$ , we need to find the  $H$  nearest inducing neighbors  $\mathbf{Z}_{\mathbf{x}_i}^H$  for  $n$  points in line 6, where  $n = |\mathcal{I}|$ ; this contributes to the worst-case complexity by  $\mathcal{O}(nMH)$ .

In line 8, we extract relevant parameters from  $\mathbf{m}$  and  $\mathbf{S}$ . We focus on the cost of extracting  $\mathbf{S}_{w(\mathbf{x}_i)}$  from  $\mathbf{S}$ . Similar to SVGP (Section 2.1), we consider  $\mathbf{S} = \mathbf{L}\mathbf{L}^T$ , where  $\mathbf{L}$  is lower triangular. We extract  $\mathbf{L}_{w(\mathbf{x}_i)} = \mathbf{D}_{w(\mathbf{x}_i)}\mathbf{L}$  which contains the rows of  $\mathbf{L}$  that correspond to the Cholesky decomposition of  $\mathbf{S}_{w(\mathbf{x}_i)} = \mathbf{L}_{w(\mathbf{x}_i)}\mathbf{L}_{w(\mathbf{x}_i)}^T$ . The computational complexity of selecting the variational parameters is  $\mathcal{O}(nMH^2)$ .

Finally, the computation of approximating the predictive distribution in line 9 requires  $\mathcal{O}(nH^3)$ . The overall complexity for SWSGP in the general case is

$\mathcal{O}(nMH + nMH^2 + nH^3)$ , which is a significant improvement over the  $\mathcal{O}(M^3)$  complexity of standard SVGP, assuming that  $n, H \ll M$ . If we choose  $\mathbf{S}$  to be diagonal, the total complexity reduces to  $\mathcal{O}(nMH + nH^3)$ ; if we additionally consider  $\mathbf{Z}$  to be fixed, the computational cost is  $\mathcal{O}(nH^3)$ . In the experiments of Section 4 we also explore these settings.

## 4 EXPERIMENTS

In this section, we conduct experiments to evaluate SWSGP on a variety of experimental conditions. We denote our approach by SWSGP-M-H, where  $M$  inducing points are used and  $H$  determines how many neighbors are selected. We introduce SVGP-M, SVGP-H and SVGP-M-H as competitors; SVGP-M and SVGP-H are using  $M$  and  $H$  inducing points, respectively. SVGP-M-H, instead, refers to SVGP using  $M$  inducing points at training time and  $H$ -nearest inducing inputs at test time.

The comparison is carried out on some UCI data sets for regression and classification, i.e., POWERPLANT, KIN8NM, NAVAL, EEG, CREDIT, and SPAM. We also consider larger scale data sets, such as MNIST and the AIRLINE data. We use the Matérn- $5/2$  kernel in all cases except for the AIRLINE dataset, where the sum of a Matérn- $3/2$  and a linear kernel is used, similar to Hensman et al. (2015). All models are trained using the Adam optimizer (Kingma and Ba, 2015) with a learning rate of 0.001 and a mini-batch size of 64. The likelihood for regression and binary classification are set to Gaussian and probit function, respectively. All models are trained over 100,000 iterations except for the AIRLINE data set where models are trained for one million iterations. In regression tasks, we report the test root mean squared error (RMSE) and the test mean negative log-likelihood (MNLL), whereas we report the test error rate (ERR) and MNLL in classification tasks. The results are averaged over three folds.

### 4.1 Increasing the number of neighbors

We begin our experimental evaluation by investigating the behavior of SWSGP with respect to  $H$ . In Figure 3, we examine SWSGP on a two-dimensional classification data set (BANANA), where  $M$  is fixed to 64 and  $H$  is increased from 4 to 64. In general, these boundaries remain sensible across the whole range of values of  $H$ , suggesting that SWSGP is able to work and converge well even though  $H$  is significantly less than  $M$ . We also observe that the contours of the classifier become smoother as  $H$  is increasing.

We then test SWSGP on other data sets with larger dimensional inputs. In these experiments,  $H$  is gradually

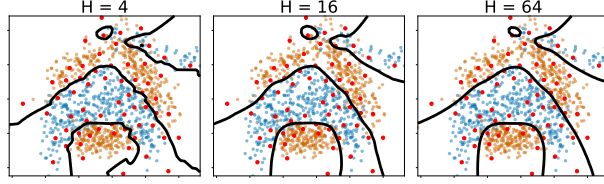


Figure 3: Visualization of SWSGP on BANANA data sets with increasing  $H$ . The total number of inducing points  $M$  is fixed to 64, while the size of neighbor area  $H$  varies from 4 to 64. The red dots represent the inducing inputs. The orange and blue dots are training points from two different classes. The black lines are the contours of a classifier where the predictive mean is 0.5.

increased to  $M$ . For POWERPLANT, KIN8NM, NAVAL, EEG, CREDIT and SPAM,  $M$  is set to 64, and for MNIST and AIRLINE,  $M$  is set to 512. In Fig. (4), we see that SWSGP-M-H consistently outperforms SVGP-M-H and SVGP-H. This suggests that including neighbor information at prediction time, combined with the use of a larger set of inducing points alone is not enough to obtain competitive performance, and that only thanks to the sparsity-inducing prior over latent variables, this yields improvements. Crucially, the performance obtained by SWSGP are comparable with those obtained by SVGP-M, while at each iteration only a subset of  $H$  out of  $M$  inducing points are updated, carrying a significant complexity reduction.

## 4.2 Increasing the number of inducing points

In this set of experiments, we show that the performance SWSGP improves when increasing the total number of inducing points, while keeping the number of active inducing points  $H$  fixed. We first illustrate this on the BANANA data set, where  $H$  is fixed to 4 and  $M$  is gradually increased from 4 to 64. In Fig. (5) we see that the classification boundaries improve when increasing  $M$ .

We also investigate the impact of increasing  $H$  and  $M$  simultaneously. In each regression and classification data set, we test SWSGP with  $H = 4, 8$  and  $M = 8, 16, 32, 64$ . The results shown in Fig. 6 indicate that using a small  $H$  is not detrimental to performance when  $M$  is large. In addition, SWSGP with a small  $H$  is comparable or better than SVGP in almost all cases.

## 4.3 Running time

We show the training and testing times of SWSGP and SVGP in Tab. 1. In SVGP, we set  $M = 256$  for POWERPLANT and KIN8NM, and 1024 for MNIST and AIRLINE, i.e. SVGP-256 and SVGP-1024. In our approach, we use

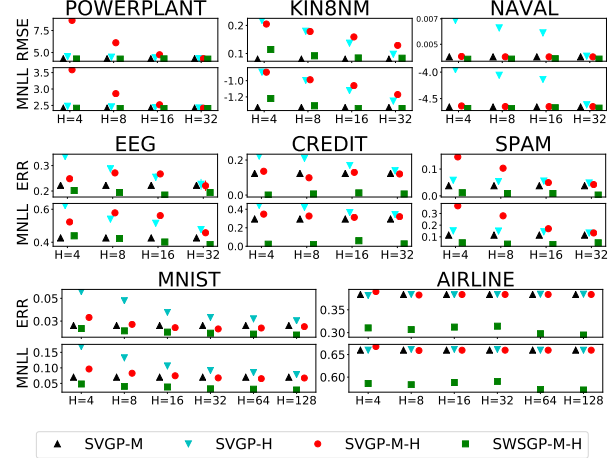


Figure 4: Evaluation of SWSGP on high-dimensional data sets with increasing  $H$ . The black up-triangles are for SVGP with  $M$  inducing points, the cyan down-triangles are for SVGP with  $H$  inducing points, the red circles are for SVGP training with  $M$  inducing points and the prediction at an unseen data  $\mathbf{x}$  are made by  $\mathbf{Z}_{\mathbf{x}}^H$ , and the green squares are for SWSGP. In these experiments,  $M$  is set to 64 and  $H$  varies from 4 to 32. Horizontal axis shows various configurations of  $H$ . The standard deviation of the error metrics over the different folds is represented by vertical bars; they are very small for most configurations.

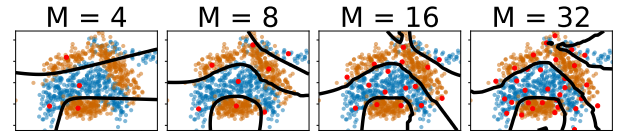


Figure 5: Visualization of SWSGP on BANANA data sets with increasing  $M$ . The size of neighbor area  $H$  is set to 4. The total number of inducing points  $M$  varies from 4 to 64. The red dots represent inducing inputs. The orange and blue dots are the input points from the two different classes. The black lines are the contours of a classifier where the predictive mean is 0.5.

the same  $M$  and we set  $H$  to 4 and  $M$ , i.e. SWSGP-256-4 and SWSGP-1024-4. Each cell of Tab. 1 follows the format of  $t_1 \mid t_2$  where  $t_1$  and  $t_2$  indicate execution time of training and testing in milliseconds. The time  $t_1$  is the averaged training time of a training iteration. The time  $t_2$  is the averaged execution time to evaluate the predictive distribution on a test point. We stress that  $t_1$  and  $t_2$  in SWSGP take into account the computation of finding neighbors inducing inputs for each data point. In SVGP, we assume that  $\mathbf{K}_{\mathbf{Z}}^{-1}$  is pre-computed and saved after the training phase. Therefore, the computational cost to evaluate the predictive distribution on a single test point is  $\mathcal{O}(M^2)$ . The time  $t_2$  in SVGP

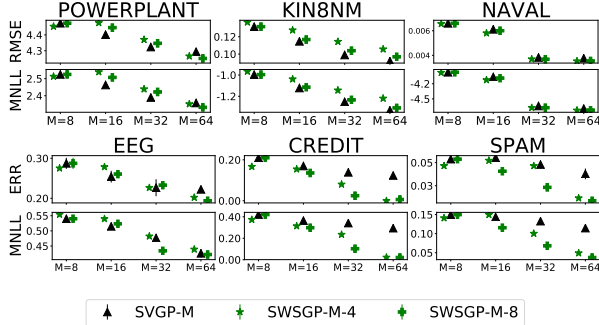
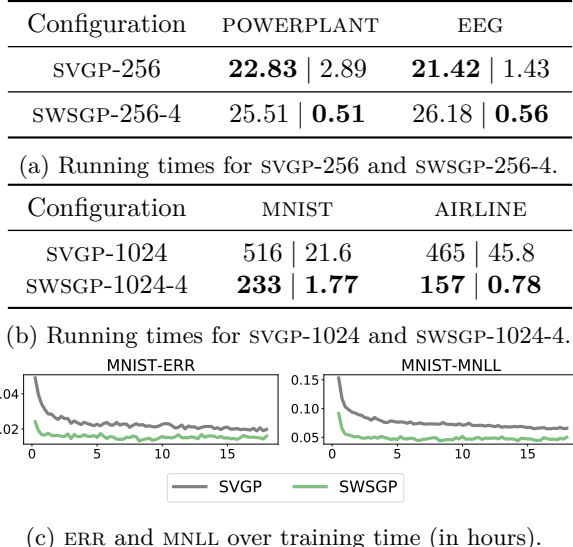


Figure 6: Evaluation of SWSGP on high-dimensional data sets with increasing  $M$ . The black up-triangles are for SVGP with  $M$  inducing points. The green stars and plus are for SWSGP with  $H$  of 4 and 8 respectively. In these experiments,  $M$  varies from 4 to 64, as shown on horizontal axes. The standard deviation of the error metrics over the different folds is represented by vertical bars; they are very small for most configurations.

Table 1: Comparison of running time between SVGP and SWSGP. In the table, each cell follows the format of [training time] | [testing time] (times are in milliseconds). In the figure, we show the progression of ERR (RMSE for regression case) and MNLL over training time. The black lines refer SVGP, and the green lines indicate SWSGP.



refers to the execution time of carrying out predictions with the complexity of  $\mathcal{O}(M^2)$ .

The results in Tab 1 show a consistent improvement at test time compared to SVGP across all values of  $H$  and  $M$ . At training time, the results show a trend dependent on the number  $M$  of inducing points. Not surprisingly, SWSGP offers limited improvements when  $M$  is small. Considering POWERPLANT and KIN8NM in

which  $M$  is set to 256, SWSGP is faster than SVGP in terms of training time. This is because the inversion of a  $256 \times 256$  matrix requires less time than finding the neighbors and inverting several  $4 \times 4$  matrices. However, Tab 1 shows dramatic speedups compared to SVGP when the number of inducing points  $M$  is large. When  $M = 1024$  on MNIST and AIRLINE, SWSGP-1024-4 is faster than SVGP-1024 in training time. This is due to the inversion of the  $1024 \times 1024$  kernel matrix being a burden for SVGP, whereas SWSGP deals with much cheaper computations. Finally, we show the progression of ERR and MNLL over training time when we train SVGP-1024 and SWSGP-1024-4 on MNIST. It becomes apparent that for large datasets our method achieves high levels of accuracy significantly more quickly in terms of running time compared to the standard SVGP.

#### 4.4 Large-scale sparse GP modeling with a huge number of inducing points

We showcase a large-scale classification problem, where we illustrate that SWSGP enables the possibility to use sparse GPs with a massive number of inducing points without incurring a prohibitive computational cost. We employ the AIRLINE data set, featuring 5 million training points. We test SWSGP with  $M = 100,000$  inducing points. We attempted to run SVGP with such a large  $M$  without success (out of memory in a system with 32GB of RAM). Therefore, as a baseline we report the results of SVGP with the configuration in Hensman et al. (2015).

In SWSGP, we impose a diagonal matrix  $\mathbf{S}$  in the variational distribution  $q(\mathbf{u} | \mathbf{w})$ , and we fix the position of the inducing inputs during training. By fixing the inducing inputs, we can operate with pre-computed information about which inducing inputs are neighbors of training inputs. Thanks to these settings, SWSGP's training phase requires  $\mathcal{O}(nH^3)$  operations only, where  $n$  is the mini-batch size. Due to the appropriate choice of  $H$  and  $n$ , and the computational cost being independent of  $M$ , unlike SVGP, we can successfully run SWSGP with  $M = 100,000$ .

By setting  $H$  and the mini-batch size  $n$  to 100 and 16 respectively, in about 24 hours of training we could run SWSGP-100,000-100 for one million iterations. The ERR and MNLL of SWSGP-100,000-100 evaluated on the test set are 21% and 0.48, respectively, while the ERR and MNLL of SVGP-200 published in Hensman et al. (2015) are about 34% and 0.61, respectively. To the best of our knowledge, SWSGP is the first to enable sparse GPs with such a large set of inducing points without imposing a grid structure on the inducing inputs.

We conclude by reporting comparisons with other GP-based models. In particular, we compare against the

Stochastic Variational Deep Kernel Learning (SVDKL) (Wilson et al., 2016) and the Deep GP approximated with random features (Cutajar et al., 2017). In the former, KISS-GP is trained on top of a deep neural network which is optimized during training, and in the latter the layers of a deep GP are approximated as parametric models using random feature expansions. Both competitors feature mini-batch-based learning, so this represents a challenging test for SWSGP. The results in Tab. 2 show that SWSGP is comparable with these competitors. We believe that this is a remarkable result obtained by our shallow SWSGP, supporting the conclusions of previous works showing that advances in kernel methods can result in performance which are competitive with deep learning approaches (see, e.g., Rudi et al. (2017)).

Table 2: Comparison of SWSGP, KISS-GP (Wilson and Nickisch, 2015), SVDKL (Wilson et al., 2016) and Deep GPs random features (Cutajar et al., 2017)

Method	RMSE	MNLL
SWSGP-64-4	<b>4.29</b>	<b>2.42</b>
KISS-GP	11.26	5.78

(a) POWERPLANT		
Method	ERR	MNLL
SWSGP-100k-100	0.21	0.48
SVDKL	0.22	0.46
Deep GP random features	0.21	0.46

(b) AIRLINE		
-------------	--	--

#### 4.5 Comparison to Local GPs

We finally demonstrate that SWSGP behaves differently from other approaches that use local approximations of GPs. We consider two well-established approaches of local GPs proposed by Kim et al. (2005) and Urtasun and Darrell (2008). Following Liu et al. (2018), we shall refer to these methods as *Inductive* GPs and *Transductive* GPs, respectively. We run all methods on two regression data sets: POWERPLANT and KIN8NM. We set the number of local experts to 64, and we use the same number of inducing points for SWSGP (with  $H$  either 4 or 8). As the size of POWERPLANT and KIN8NM are approximately 7000, we set the number of training points governed by a local expert to 100. For the local GP approaches, we choose 64 locations in the input space using the  $K$ -means algorithm, and for each location we choose 100 neighboring points; we then train the corresponding local GP expert. Regarding the testing phase, inductive GPs simply rely on the nearest local experts to an unseen point  $\mathbf{x}_*$ . Whereas for transductive GPs, we use 100 neighbors of  $\mathbf{x}_*$  and

the nearest local expert to make predictions. In table 3, we summarize RMSE and MNLL for all methods; SWSGP clearly outperforms the local GP approaches in terms of MNLL.

Table 3: Comparison with Local GP approximations.

Method	POWERPLANT		KIN8NM	
	RMSE	MNLL	RMSE	MNLL
SWSGP-64-4	4.27	2.41	0.11	-1.27
SWSGP-64-8	<b>4.24</b>	<b>2.40</b>	0.10	<b>-1.38</b>
Inductive GPs	9.93	38.38	0.13	-0.40
Transductive GPs	6.17	18.78	<b>0.09</b>	-0.65

## 5 CONCLUSIONS

Sparse approaches that rely on inducing points have met with success in reducing the complexity of GP regression and classification. However, these methods are limited by the number of inducing inputs that is required to obtain an accurate approximation of the true GP model. A large number of inducing inputs is often necessary in cases of very large datasets, which marks the limits of practical applications for most GP-based approaches.

In this work, we further improve the computational gains of sparse GPs. We proposed SWSGP, a novel methodology that imposes a hierarchical and sparsity-inducing effect on the prior over the inducing variables. This has been realized as a conditional GP given a random subset of the inducing points, which is defined as the nearest neighbors of random mini-batches of data. We have developed an appropriate variational bound which can be estimated in an unbiased way by means of mini-batches. We have performed an extensive experimental campaign that demonstrated the superior scalability properties of SWSGP compared to the state-of-the-art.

## References

- D. Burt, C. E. Rasmussen, and M. Van Der Wilk. Rates of convergence for sparse variational Gaussian process regression. In *Proceedings of the 36th International Conference on Machine Learning*, volume 97 of *Proceedings of Machine Learning Research*, pages 862–871. PMLR, 2019.
- L. Csató and M. Opper. Sparse on-line gaussian processes. *Neural Computation*, 14(3):641–668, 2002. ISSN 0899-7667.
- K. Cutajar, E. V. Bonilla, P. Michiardi, and M. Filippone. Random feature expansions for deep Gaussian

processes. In *Proceedings of the 34th International Conference on Machine Learning*, volume 70 of *Proceedings of Machine Learning Research*, pages 884–893. PMLR, 2017.

A. Datta, S. Banerjee, A. Finley, and A. Gelfand. On nearest-neighbor gaussian process models for massive spatial data: Nearest-neighbor gaussian process models. *Wiley Interdisciplinary Reviews: Computational Statistics*, 8, 08 2016.

J. Hensman, N. Fusi, and N. D. Lawrence. Gaussian processes for big data. In *Proceedings of the 29th Conference on Uncertainty in Artificial Intelligence*, pages 282–290. AUAI Press, 2013.

J. Hensman, A. Matthews, and Z. Ghahramani. Scalable Variational Gaussian Process Classification. In *Proceedings of the 18th International Conference on Artificial Intelligence and Statistics*, volume 38 of *Proceedings of Machine Learning Research*, pages 351–360. PMLR, 2015.

H.-M. Kim, B. Mallick, and C. Holmes. Analyzing nonstationary spatial data using piecewise gaussian processes. *Journal of the American Statistical Association*, 100:653–668, 02 2005.

D. P. Kingma and J. Ba. Adam: A method for stochastic optimization. In *3rd International Conference on Learning Representations*, 2015.

N. D. Lawrence, M. Seeger, and R. Herbrich. Fast Sparse Gaussian Process Methods: The Informative Vector Machine. In *Advances in Neural Information Processing Systems 15*, pages 625–632. MIT Press, 2002.

H. Liu, Y. Ong, X. Shen, and J. Cai. When gaussian process meets big data: A review of scalable gps, 07 2018.

C. Louizos, K. Ullrich, and M. Welling. Bayesian compression for deep learning. In *Advances in Neural Information Processing Systems 30*, pages 3288–3298. Curran Associates, Inc., 2017.

D. Molchanov, A. Ashukha, and D. Vetrov. Variational dropout sparsifies deep neural networks. In *Proceedings of the 34th International Conference on Machine Learning*, volume 70 of *Proceedings of Machine Learning Research*, pages 2498–2507. PMLR, 2017.

A. Naish-Guzman and S. Holden. The generalized FITC approximation. In *Advances in Neural Information Processing Systems 20*, pages 1057–1064. Curran Associates Inc., 2007. ISBN 978-1-60560-352-0.

A. Panos, P. Dellaportas, and M. K. Titsias. Fully Scalable Gaussian Processes using Subspace Inducing Inputs. 2018. arXiv:1807.02537.

C. Park and D. Apley. Patchwork kriging for large-scale gaussian process regression. *Journal of Machine Learning Research*, 19, 01 2017.

C. Park and J. Z. Huang. Efficient computation of gaussian process regression for large spatial data sets by patching local gaussian processes. *J. Mach. Learn. Res.*, 17(1):6071–6099, Jan. 2016. ISSN 1532-4435.

G. Pleiss, J. Gardner, K. Weinberger, and A. G. Wilson. Constant-time predictive distributions for Gaussian processes. In *Proceedings of the 35th International Conference on Machine Learning*, volume 80 of *Proceedings of Machine Learning Research*, pages 4114–4123. PMLR, 2018.

A. Pourhabib, F. Liang, and Y. Ding. Bayesian site selection for fast Gaussian process regression. *Institute of Industrial Engineers Transactions*, 46(5):543–555, 2014.

J. Quiñonero Candela and C. E. Rasmussen. A unifying view of sparse approximate Gaussian process regression. *Journal of Machine Learning Research*, 6:1939–1959, 2005. ISSN 1532-4435.

C. E. Rasmussen and C. Williams. *Gaussian Processes for Machine Learning*. MIT Press, 2006.

A. Rudi, L. Carratino, and L. Rosasco. FALKON: An Optimal Large Scale Kernel Method. In *Advances in Neural Information Processing Systems 30*, pages 3888–3898. Curran Associates, Inc., 2017.

M. Seeger, C. K. I. Williams, and N. D. Lawrence. Fast forward selection to speed up sparse Gaussian process regression. In *Artificial Intelligence and Statistics 9*, 2003.

E. Snelson and Z. Ghahramani. Sparse Gaussian Processes using Pseudo-inputs. In *Advances in Neural Information Processing Systems 18*, pages 1257–1264. MIT Press, 2005.

M. K. Titsias. Variational Learning of Inducing Variables in Sparse Gaussian Processes. In *Proceedings of the 12th International Conference on Artificial Intelligence and Statistics*, volume 5 of *Proceedings of Machine Learning Research*, pages 567–574. PMLR, 2009.

R. Urtasun and T. Darrell. Sparse probabilistic regression for activity-independent human pose inference. In *2008 IEEE Conference on Computer Vision and Pattern Recognition*, pages 1–8, 2008.

A. Wilson and H. Nickisch. Kernel Interpolation for Scalable Structured Gaussian Processes (KISS-GP). In *Proceedings of the 32nd International Conference on Machine Learning*, volume 37 of *Proceedings of Machine Learning Research*, pages 1775–1784. PMLR, 2015.

A. G. Wilson, C. Dann, and H. Nickisch. Thoughts on Massively Scalable Gaussian Processes. 2015. arXiv:1511.01870.

A. G. Wilson, Z. Hu, R. R. Salakhutdinov, and E. P. Xing. Stochastic Variational Deep Kernel Learning. In D. D. Lee, M. Sugiyama, U. V. Luxburg, I. Guyon, and R. Garnett, editors, *Advances in Neural Information Processing Systems 29*, pages 2586–2594. Curran Associates, Inc., 2016.